Picolinic acid based Cu(II) complexes with heterocyclic bases – Crystal structure, DNA binding and cleavage studies

ARTICLE *in* EUROPEAN JOURNAL OF MEDICINAL CHEMISTRY · APRIL 2014

Impact Factor: 3.45 · DOI: 10.1016/j.ejmech.2014.03.084 · Source: PubMed

4 AUTHORS, INCLUDING:

Raju Nomula
Osmania University
12 PUBLICATIONS **83** CITATIONS
SEE PROFILE

Raghavaiah Pallepogu
Dr. Harisingh Gour University
84 PUBLICATIONS **649** CITATIONS
SEE PROFILE

European Journal of Medicinal Chemistry 79 (2014) 117–127

Contents lists available at ScienceDirect

European Journal of Medicinal Chemistry

journal homepage: http://www.elsevier.com/locate/ejmech

Original article

Picolinic acid based Cu(II) complexes with heterocyclic bases – Crystal structure, DNA binding and cleavage studies

Rabindra Reddy Pulimamidi [a,*], Raju Nomula [a], Raghavaiah Pallepogu [b], Hussain Shaik [a]

[a] Department of Chemistry, Osmania University, Hyderabad 500007, India
[b] School of Chemistry, University of Hyderabad, Hyderabad 500046, India

ARTICLE INFO

Article history:
Received 11 November 2013
Received in revised form
27 January 2014
Accepted 31 March 2014
Available online 1 April 2014

Keywords:
Picolinic acid
Copper(II) complexes
Crystal structure
DNA binding
DNA cleavage

ABSTRACT

In view of the importance of picolinic acid (PA) in preventing cell growth and arresting cell cycle, new PA based metallonucleases were designed with a view to study their DNA binding and cleavage abilities. Three new Cu(II) complexes [Cu(II)(DPPA)].4H_2O (**1**),[Cu(II)(DPPA)(bpy)].5H_2O (**2**) and [Cu(II)(DPPA)(-phen)].5H_2O (**3**), were synthesized using a picolinic acid based bifunctional ligand (DPPA) and heterocyclic bases (where DPPA: Pyridine-2-carboxylic acid {2-phenyl-1-[(pyridin-2-ylmethyl)-carbonyl]-ethyl}-amide; bpy: 2, 2′-bipyridine and phen: 1, 10-phenanthroline). DPPA was obtained by coupling 2-picolinic acid and 2-picolyl amine with L-phenylalanine through amide bond. Complexes were structurally characterized by a single crystal X-ray crystallography. The molecular structure of **1** shows Cu(II) center essentially in a square planar coordination geometry, while complex **2** shows an approximate five coordinated square-pyramidal geometry. Eventhough we could not isolate single crystal for complex (**3**), its structure was established based on other techniques. The complex (**3**) also exhibits five coordinate square pyramidal geometry. The complexes show good binding affinity towards CT-DNA. The binding constants (K_b) decrease in the order $1.35 \pm 0.01 \times 10^5$ (**3**) > $1.23 \pm 0.01 \times 10^5$ (**2**) > $8.3 \pm 0.01 \times 10^4$ (**1**) M^{-1}. They also exhibit efficient nuclease activity towards supercoiled pUC19 DNA both in the absence and presence of external agent (H_2O_2). The kinetic studies reveal that the hydrolytic cleavage reactions follow the pseudo first-order rate constant and the hydrolysis rates are in the range of (5.8–8.0) $\times 10^7$ fold rate enhancement compared to non-catalyzed double stranded DNA (3.6×10^{-8} h^{-1}).

1. Introduction

The interaction of metal complexes with DNA is of great interest for the development of artificial endonucleases followed by anticancer drug therapies. DNA offers several potential binding sites for transition metals, including the anionic phosphate backbone, electron-rich bases, and the major or minor grooves [1]. Transition metal complexes can associate with DNA mainly in two types of binding motifs: Covalent and non-covalent binding (intercalation, electrostatic interaction and major/minor groove binding). The well-studied first generation anticancer complex, cisplatin [cis-$Pt(NH_3)_2Cl_2$], binds covalently to the N^7-guanine of DNA, causing a distortion to the structure of DNA double helix leading to serious side effects and cell death [2–5]. Because of this, the usage of cisplatin is limited. Hence, other metals like copper [6–8], and ruthenium [9–11] are now regarded as promising alternatives to platinum in cancer therapy. Copper is most abundant bio-essential element with two oxidation states (+1 and +2) which are important in most aerobic organisms, is employed as a structural and catalytic cofactor, and consequently it is involved in many biological pathways [12]. The coordination flexibility and distortion ability of Cu(II) complexes contribute significantly to the structural diversity, which eventually play a vital role in DNA binding and cleavage.

Nitrogen ligands have been extensively used in coordination chemistry [13,14], especially to obtain derivatives that are able to mimic structural, spectroscopic and catalytic features of active sites of metallo-enzymes [15–18]. As a typical heterocyclic planar ligands, 1,10-phenanthroline and 2,2-bipyridine have attracted attention due to their diverse and wide-ranging antiviral, photochemical and photophysical properties, versatile coordination modes and the potential to form supramolecular aggregates through π…π stacking interactions. Thus, the design of their metal complexes have continuously increased since many of these materials may serve as models which mimic both the structure and reactivity of metal ion sites in complex biological systems and possess a broad spectrum of biological activity [19–21].

* Corresponding author.
E-mail addresses: rabi_pr@rediffmail.com, profprreddy@gmail.com (R. R. Pulimamidi).

http://dx.doi.org/10.1016/j.ejmech.2014.03.084
0223-5234/

Many useful applications of the complexes require that the complexes bind to DNA through intercalative mode since it is one of the important binding modes that invariably lead to cellular degradation [22]. Considering the prominent role of intercalators in enhancing DNA binding, cleavage and biological applications, we have been focusing our attention in the development of new metallonucleases with increased ligand aromaticities [23–30]. Recently, it was shown that the treatment with picolinic acid disordered the cell growth and arrested cell cycle [31]. Picolinic acid also stimulates programmed cell-death (PCD) in cancer cells and efficiently interrupts the progress of HIV in vitro [32]. In view of this, we have synthesized a picolinic acid based ligand (DPPA), with phenylalanine and picolyl amine [33] and isolated its binary and ternary copper complexes. We reported (Fig. 1) herein the synthesis, characterization and X-ray structure (**1** & **2**). In the absence of crystal structure for (**3**), the geometry was established based on other techniques. Their interaction with CT-DNA was studied by employing various biophysical techniques such as thermal denaturation, electronic absorption, viscosity and fluorescence spectroscopy. The binding constants (K_b) for these complexes were determined ($1.35 \pm 0.01 \times 10^5$ (**3**), $1.23 \pm 0.01 \times 10^5$ (**2**) and $8.3 \pm 0.01 \times 10^4$ (**1**) M^{-1}). The DNA cleavage activity of the complexes was evaluated using gel electrophoresis technique. They bind and cleave DNA efficiently. The DNA hydrolysis rate constants were also determined. The ternary complexes (**2**, **3**) bind and cleave DNA more efficiently compared to binary complex (**1**).

Table 1
Important crystallography data of complexes **1** and **2**.

	1	**2**
CCDC	788099	811860
Formula	$C_{21}H_{18}$ Cu N_4 O_5.50	$C_{31}H_{36}$ Cu N_6 O_7
M	477.93	668.20
Cryst syst	Monoclinic	Monoclinic
T (K)	293(2)	293(2)
Wavelength/Å	0.71073	0.71073
Space group	C 1 2/c 1	P2(1)/c
a/Å	23.382 (5)	11.2413 (7)
b/Å	14.6449 (17)	23.3226 (15)
c/Å	13.904 (2)	13.3537 (9)
α (deg)	90	90
β (deg)	114.38 (2)	114.2790 (10)
γ (deg)	90	90
V/Å^3	4336.6 (12)	3191.4 (4)
Z	8	4
D_c/mgm^{-3}	1.464	1.391
Absorption coefficient/min^{-1}	1.050	0.740
F (000)	1960	1396
Crystal size/mm^3	0.42 × 0.30 × 0.14	
θ range for data collection (deg)	2.78 to 26.37	1.75 to 26.02
Reflections collected	9974	24640
Independent reflections	4435 [*R*(int) = 0.0412]	6258 [*R*(int) = 0.0495]
Completeness to $\theta = 26.37$	99.9	99.6
Max. and min. transmission	0.8670 and 0.6669	0.9297 and 0.8196
Data/restraints/parameters	4435/0/286	6258/9/446
Goodness-of-fit on F^2	0.914	1.262
Largest diff. peak and hole (e Å^{-3})	0.584 and −0.325	0.538 and −0.530

2. Experimental part

2.1. Materials

Picolinic acid, picolyl amine, phenylalanine-methyl ester, DCC (*N*,*N*′-dicyclohexyl carbodiimide), 2, 2′-bipyridine (bpy), 1, 10-phenanthroline (phen), $Cu(OAc)_2.H_2O$, $LiOH.H_2O$ and ethidium bromide (EB) were obtained from Sigma (99.99% purity) USA and were of analar grade. Solvents (MeOH, EtOH, CH_2Cl_2) were purchased from Merck, India. The CT-DNA was obtained from Fluka (Switzerland), supercoiled pUC19 DNA, agarose, tris-base and tris–HCl were obtained from Bangalore Genei (India). The chemicals were used as supplied.

2.2. Methods

Elemental analyses were obtained from the microanalytical Heraeus Carlo Elba 1108 elemental analyzer. The molar conductivity was measured on a Digisun digital conductivity bridge (model: DI-909) with a dip type cell. NMR spectra obtained from Bruker biospin Avance-III 400 MHz spectrometer. Infrared spectra were recorded on a Perkin–Elmer FT-IR spectrometer, in KBr pellets in the 4000–400 cm^{-1} range. Magnetic susceptibilities of the complexes were recorded at room temperature on a Faraday balance (CAHN-7600) using Hg[Co(NCS)$_4$] as the internal standard. Diamagnetic corrections were made by using Pascal's constants [34]. ESI mass spectra of the complexes were recorded using a Quattro Lc (Micro mass, Manchester, UK) triple quadruple mass spectrometer with Mass Lynx software. UV–vis spectra of the complexes were recorded on a Shimadzu 160A spectrophotometer (800–200 nm) and Jasco V-530 UV–**v**is spectrophotometer using 1-cm quartz micro-cuvettes. Gel pattern after the electrophoresis was photographed by Alpha-Innotec gel documentation system (USA).

2.3. X-ray crystallographic procedures

Reddish brown single crystals of **1** and **2** were grown by slow evaporation of reaction solution (aq.MeOH) for a week at room temperature. A crystal of the complex was mounted on a glass fiber and used for data collection. Crystal data were collected at 293 K, using Bruker-Nanious SMART APEX CCD single crystal diffractometer equipped with a graphite monochromator and a Mo Kα fine-focus sealed tube ($\lambda = 0.71073$ Å) operated at 2.0 kW. The detector was placed at a distance of 6.0 cm from the crystal. Data were collected with a scan width of 0.3° in ω and an exposure time of 15 s/frame. The SMART software was used for data acquisition and

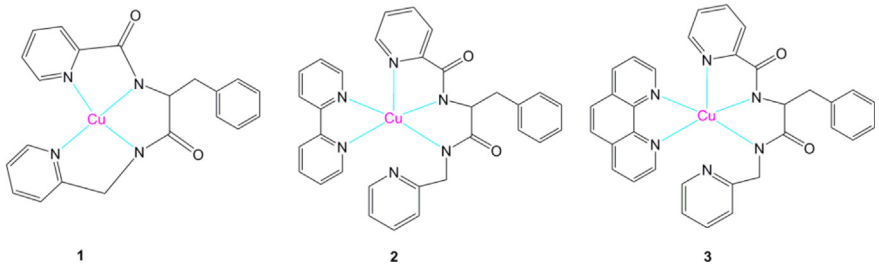

Fig. 1. Proposed structures of the complexes **1**–**3**.

the SAINT-Plus software was used for data extraction [35]. The absorption corrections were performed with the help of SADABS program [36] The SHELX-97 programs [37] available in the WinGX package [38] was used for structure solution and refinement. The ORTEX6a [39] and Platon [40] packages were used for molecular graphics. All the non-hydrogen atoms were refined with anisotropic displacement parameters. All the hydrogen atoms could be located in Difference Fourier map. However, they were relocated at chemically meaning full positions and were given riding model refinement. The refinement of water hydrogen atoms were restrained such that they remain in the vicinity of the respective difference peak. The selected crystallographic data of **1** and **2** was given in Table 1.

2.4. Syntheses of ligand (DPPA) and complexes (*1*–*3*)

The ligand **DPPA** was synthesized as per the literature [33]. This is described schematically in Scheme 1. The **PA-I**, **PA-II** and the final ligand (**DPPA**) were isolated and characterized. The details are provided in Supplementary Information†.

The ligand **DPPA** (0.36 g; 1 mmol) was dissolved in methanol (10 mL) and added drop wise to an aq. methanolic solution (10 mL) of $Cu(OAC)_2$. H_2O (0.198 g; 1 mmol). The solution was stirred for 6 h at room temperature to obtain complex **1**. Complex **1** (0.421 g; 1 mmol) was dissolved in aq. methanol (10 mL) and to this a methanolic solution (15 mL) of bpy (0.156 g; 1 mmol)/phen (0.198 g; 1 mmol) was added and stirring was continued for 3 h to afford **2** and **3** respectively (Scheme 1). The reaction solutions were kept for slow evaporation for few days to isolate single crystals. Reddish brown crystals were obtained for **1** and **2**. A brown solid was isolated for complex **3**.

2.4.1. *[1]*

Yield: (0.357 g, 85%). Elemental analyses: (Found: C, 50.70; H, 5.27; N, 11.20. Calc. for $C_{21}H_{26}CuN_4O_6$: C, 51.06; H, 5.30; N, 11.34%). ESI-MS: *m/z* 422 ($M^+ + H$, 100%), 444 ($M^+ + Na$, 34%). UV–vis: λ_{max} (H_2O:MeOH, 9:1)/nm: 257, 393, 530. IR: ν_{max}/cm^{-1}: 3438br (OH), 2927w (CH), 1643vs (C=O), 1599s (C=C), 1404 (C=N), 1051, 824, 765, 690, 520w (Cu–N). μ_{eff} = 1.69 B M. Λ_M [Ω^{-1} cm^2 mol^{-1}, 10^{-3} M in aq. methanol, 25 °C] = 4.60.

2.4.2. *[2]*

Yield: (0.404 g, 70%). Elemental analyses: (Found: C, 55.47; H, 5.39; N, 12.33. Calc. for $C_{31}H_{36}CuN_6O_7$: C, 55.72; H, 5.43; N, 12.58%). ESI-MS: *m/z* 578 ($M^+ + H$, 85%). UV–vis: λ_{max} (H_2O:MeOH, 9:1)/nm: 207, 270, 392, 690. IR: ν_{max}/cm^{-1}: 3425br (OH), 2926w, 2862w (CH), 1615vs (C=O), 1596s (C=C), 1404s (C=N), 1339, 1292, 1157, 1084, 1023, 823, 764, 695, 580 m (Cu–N). μ_{eff} = 1.73 B M. [Ω^{-1} cm^2 mol^{-1}, 10^{-3} M in aq. methanol, 25 °C] = 12.40.

2.4.3. *[3]*

Yield: (0.420 g, 70%). Elemental analyses: (Found: C, 56.92; H, 5.19; N, 12.03. Calc. for $C_{33}H_{36}CuN_6O_7$: C, 57.26; H, 5.24; N, 12.14%). ESI-MS: *m/z* 602 ($M^+ + H$, 100%), 624 ($M^+ + Na$, 28%). UV–vis: λ_{max} (H_2O:MeOH, 9:1)/nm: 222, 264, 395, 710. IR: ν_{max}/cm^{-1}: 3427br (OH), 3079, 2925, 2861w (CH), 1618vs (C=O), 1594s (C=C), 1428s (C=N), 1343, 1082, 850, 770, 730, 583 m (Cu–N). μ_{eff} = 1.80 B M. [Ω^{-1} cm^2 mol^{-1}, 10^{-3} M in aq. methanol, 25 °C] = 15.70.

2.5. DNA binding

2.5.1. Preparation of stock solutions

Concentrated CT-DNA stock solution was prepared in 5 mM tris–HCl/50 mM NaCl in double distilled water at pH = 7.5 and the concentration of DNA solution was determined by UV absorbance at 260 nm (ε = 6600 M^{-1} cm^{-1}) [41]. Solution of CT-DNA in 5 mM tris–HCl/50 mM NaCl (pH = 7.5) gave a ratio of UV absorption at 260 nm and 280 nm A_{260}/A_{280} of ca. 1.8–1.9, indicating that the DNA was sufficiently free of protein contamination [42]. The concentration of EB solution was determined spectrophotometrically at 480 nm (ε = 5680 M^{-1} cm^{-1}) [43]. All stock solutions were stored at 4 °C and were used within couple of days. All DNA binding and cleavage experiments were carried out in tris buffer. The stock solutions of metal complexes were prepared in water methanol (9:1) mixture.

Based on competitive binding experiments, it was concluded that the saturation of binding reaches when the concentration of reacting species (DNA & complexes) are in an equimolar (1:1) ratio. Accordingly all the measurements were performed only up to that ratio. The major species present at the medium of interaction were either 1:1 or 1:1:1 for binary and ternary complexes respectively.

2.5.2. Thermal denaturation studies

The thermal denaturation studies were performed on Shimadzu 160A spectrophotometer equipped with a thermostatic cell holder. DNA (30 μM) was treated with complexes **1**–**3** (30 μM) in a 1:1 ratio in tris buffer at pH 7.5. The samples were continuously heated at the rate of 1 °C min^{-1} while monitoring the absorption changes at 260 nm. The melting temperature (T_m) and the melting interval (ΔT_m) data were obtained from the experiment as per the reported procedure [44].

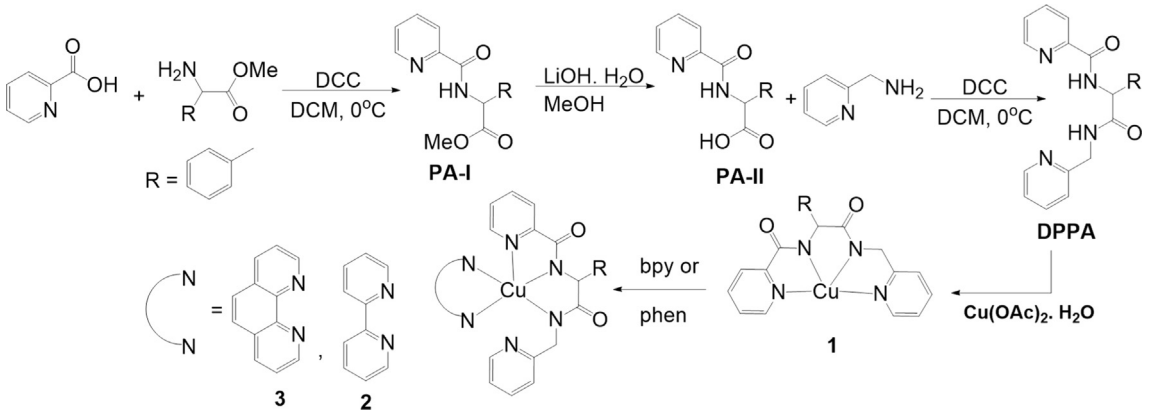

Scheme 1. Syntheses of complexes **1**–**3**.

*2.5.3. Interaction of CT DNA with **1**–**3** by UV–vis titration*

Absorption spectra were recorded on Jasco V-530 UV–visible spectrophotometer using 1-cm quartz micro-cuvettes. Absorption titrations were performed by keeping the concentration of the complexes (**1**–**3**) constant (10 μM) and monitored the charge transfer bands absorbance changes upon increasing the concentration of CT-DNA from 0 to 10 μM. In the reference cell, a blank DNA was placed so as to nullify the DNA absorbance at measured wavelength. For the complexes **1**–**3**, the binding constants (K_b) were determined from the spectroscopic titration data using the following equation [45,46].

$$[DNA]\Big/\left(\varepsilon_a - \varepsilon_f\right) = [DNA]\Big/\left(\varepsilon_b - \varepsilon_f\right) + 1\Big/K_b\left(\varepsilon_b - \varepsilon_f\right) \quad (1)$$

The 'apparent' extinction coefficient (ε_a) was obtained by calculating A_{obsd}/[Cu]. The terms ε_f and ε_b correspond to the extinction coefficients of free (unbound) and the fully bound complexes, respectively. From a plot of [DNA]/($\varepsilon_a - \varepsilon_f$) Versus [DNA] will give a slope 1/($\varepsilon_b - \varepsilon_f$) and an intercept 1/$K_b$($\varepsilon_b - \varepsilon_f$). K_b is the ratio of the slope to the intercept.

2.5.4. Viscosity

Viscometric titrations were performed with an Ostwald Viscometer at room temperature. The concentration of DNA was 200 μM, complex concentration was varied from 0 to 200 μM and the flow times were measured with a digital timer. Each sample was measured three times for accuracy, and an average flow time was determined. Data was presented as $(\eta/\eta_o)^{1/3}$ vs. [complex]/[DNA], where η is the viscosity of DNA in the presence of complex and η_o that of DNA alone. Viscosity values were calculated from the observed flow time of DNA containing solutions (t) corrected for that buffer alone (5 mM tris HCl/50 mM NaCl) (t_o), $\eta = (t - t_o)$.

2.5.5. Competitive binding

These experiments were also performed on Jasco V-530 UV–visible spectrophotometer using 1-cm quartz micro-cuvettes. Absorption titrations were performed for **1**–**3** complexes by keeping the concentration of the EB (40 μM), DNA (40 μM) constant, and by varying complex concentration from 0 to 40 μM.

2.5.6. Fluorescence spectra

Fluorescence spectra were recorded with SPEX- Fluorolog 0.22 m fluorimeter equipped with a 450 W Xenon lamp. The slit widths were 2 × 2 × 2 × 2 and the emission spectral range was 550–650 nm. Solution containing DNA and EB was titrated with varying concentrations of **1**–**3**. The concentration of DNA and EB was maintained at 41 μM and the concentration of complexes was in the range of 0–196 μM. The solutions containing DNA and EB were mixed in an equimolar ratio and the complexes **1**–**3** were added and allowed to equilibrate till a clear solution was obtained. They were excited at 540 nm (λ_{max} for EB) and the fluorescence emission at 598 nm (λ_{max}) was recorded.

Fluorescence spectra were also utilized to obtain *Scatchard* plots. For this, titration of DNA against EB in the absence and presence of copper complexes were performed. Initial concentration of DNA in tris buffer is 20 μM and the concentrations of **1**–**3** were kept at 50 μM. After each addition of EB to the solutions containing DNA and copper complexes, the emission spectra were recorded in the range of 550–650 nm with excitation at 540 nm at 25 °C. Corrections were made to the data for the volume changes during the course of titrations. The data were analyzed by the method of Lepecq and Paoletti [47] to obtain bound (c_b) and free (c_f) concentration of EB and *Scatchard* plots were obtained by plotting r_{EB}/c_f Vs r_{EB} (where $r = c_b$/conc. of DNA).

2.6. DNA cleavage

Electrophoresis experiments were performed using supercoiled pUC19 plasmid DNA (SC DNA) in accordance with the established procedures. The cleavage of SC DNA (38 μM base pair concentration) was accomplished by the addition of Cu(II) complexes in the absence (0–150 μM, 0–80 μM and 0–60 μM of **1**–**3**, respectively) and presence (0–15 μM of **1** and 0–5 for **2** & **3**) of 1 mM H_2O_2. The total volume of the solution was maintained constant at 16 μL by adding 5 mM tris buffer. The mixtures were incubated at 37 °C for a period of 2 h. The reactions were quenched and the resulting solutions were subjected to electrophoresis. The analysis involved loading of the solutions onto 1% agarose gels containing 2.5 μM EB (2 μL), and the DNA fragments separated by gel electrophoresis (60 V for 2 h in standard tris-acetate-EDTA (TAE) buffer, pH 8). Ethidium-stained agarose gels were imaged, and densitometric analysis of the visualized bands was used to determine the extent of DNA cleavage.

Control experiments were carried out using $Cu(OAc)_2.H_2O$, free ligands at a concentration of 1 mM. In order to gain an insight into the mechanism of hydrolytic cleavage: the cleavage of SC DNA (38 μM base-pair concentration of SC DNA) was carried out at a concentration of 150, 80, 60 μM of complexes **1**–**3** respectively in the presence of 1 mM DMSO, a known hydroxyl radical scavenger. For oxidative cleavage, the concentration of complexes was 15 μM for **1** and 5 μM for **2** & **3** in the presence of 1 mM DMSO and 1 mM H_2O_2. Each solution was incubated at 37 °C for 2 h and analyzed by the procedure described above. For evaluating kinetic data, the complex concentration was fixed at 100 μM with different incubation times (0–60 min) under identical experimental conditions.

3. Results and discussion

The complexes were soluble in water methanol mixture (9:1). They were non-hygroscopic and stable in both solid and solution phases. The analytical data for the complexes are in good agreement with their formulations. The molar conductance values are too low to account for any dissociation of the complexes in aq.MeOH, suggesting the non-electrolytic nature of the complexes. The observed magnetic moment values for **1**–**3** in the range of

Table 2
Physico-chemical data for complexes **1**–**3**.

Complex	IR (cm^{-1})[a] υ(Cu–N)	μ_{eff}[b] (BM)	ESI-MS (*m*/*z*)	UV–vis[c] (nm)	Λ_M[d] (Ω^{-1} Cm^2 M^{-1})
(**1**)	578	1.69	422	530, 393, 257	4.60
(**2**)	516	1.73	578	690, 392, 270, 207	12.40
(**3**)	583	1.80	602	710, 395, 264, 222	15.70

[a] IR (KBr phase, cm^{-1}).
[b] Magnetic moment (BM).
[c] UV-visible spectra in H_2O:MeOH (λ_{max}/nm).
[d] Molar conductance in MeOH (Ω^{-1} Cm^2 M^{-1}).

1.69–1.80 BM are suggestive of one unpaired electron system with spin (1/2), which represents the paramagnetic nature of Cu(II) complexes [48]. Important physico-chemical data for **1**–**3** were obtained and tabulated in Table 2.

Reddish brown crystals were isolated for complexes **1** and **2** by slow evaporation of reaction solutions for few days at room temperature. In spite of trying in different conditions and solvents, we could not succeed in isolating single crystals for **3**. However, the complexes were comprehensively characterized by various established physico-chemical techniques.

3.1. Crystal structure description of *1*

The ortep diagram of the complex **1** is shown in Fig. 2a and selected bond distances and angles were given in Table 3. The complex **1** is in monoclinic system with space group C12/c1 and the copper center lies in an N4 coordination environment with four lattice water molecules for **1**. The ligand **DPPA** coordinates with Cu(II) ion in a tetra-dentate manner utilizing N atoms of two different functions, namely amidate (deprotonated amide) (N1 and N2) and pyridine (N3 and N4) as potential donor sites in **1** resulting in the formation of three five membered chelating rings (CuNCCN). The bond distances from metal center to donor sites are Cu(1)–N(1) 1.893(3), Cu(1)–N(2) 1.916(3), Cu(1)–N(3) 2.013(3) and Cu(1)–N(4) 2.027(3) respectively. The pyridyl N-atoms are slightly elongated from the ideal M–N bond distances. The bond angles around the Cu(II) are not orthogonal at 82.60(13), 82.68(12), 82.45(11), and 112.24(12) for each N(1)–Cu(1)–N(2), N(1)–Cu(1)–N(3), N(2)–Cu(1)–N(4) and N(3)–Cu(1)–N(4)1 respectively are slightly deviated from 90°. However the sum of the angles around Cu(II) is very close to 360° indicating a planar geometry. Therefore, the coordination geometry around Cu(II) is slightly distorted from ideal square-planar as elucidated by bond angles and inter planar angles around the metal atom, which are composed of three five membered chelating rings (CuNCCN) in complex **1**. Dihedral angle [°] between the least-square planes (N1–Cu–N2) and (N3–Cu–N4) = 2.090(1)° is a measure of deviation from square-planarity.

3.2. Crystal structure description of *2*

Similarly, the complex **2** is also a monoclinic system with P2(1)/c space group. The ortep diagram (Fig. 2b) of **2** shows N5 coordination with approximate square pyramidal geometry around the copper center. In this complex DPPA acts as a tri-dentate ligand in contrast to its tetra-dentate nature with Cu(1)–N(1) 2.043(3), Cu(1)–N(2) 1.928(3) and Cu(1)–N(3) 1.956(3) bond distances (Table 3), and occupying three equatorial positions of basal plane of the square. The secondary ligand bpy occupies one equatorial and one axial position with Cu(1)–N(5) 2.032(3) and Cu(1)–N(6) 2.255(3) bond distances respectively. The Cu–N axial distance is elongated with respect to the Cu–N basal distances by 0.20 is typical for d^9 Cu(II) centers with a square pyramidal geometry. The bond angles between two coordinates in square are 81.89(13), 95.29(13), 82.54(12) and 96.95(12) for each N(1)–Cu(1)–N(2), N(1)–Cu(1)–N(5), N(2)–Cu(1)–N(3) and N(3)–Cu(1)–N(5) respectively. The sum of the square angles is 356.67° which is slightly deviated from ideal square (360°). The axial nitrogen (N6) also show small angle towards N(1)–Cu(1)–N(5) plane compared to other planes due to the rigidity of the bpy molecule. This also accounts for the distortion in the geometry.

Table 3
Important bond lengths and bond angles of **1** and **2**.

(**1**)		(**2**)	
Bond lengths	Bond angles	Bond lengths	Bond angles
Cu(1)–N(1) 1.893(3)	N(1)–Cu(1)–N(2) 82.60(13)	Cu(1)–N(1) 2.043(3)	N(1)–Cu(1)–N(2) 81.89(13)
Cu(1)–N(2) 1.916(3)	N(1)–Cu(1)–N(3) 82.68(12)	Cu(1)–N(2) 1.928(3)	N(1)–Cu(1)–N(3) 60.05(12)
Cu(1)–N(3) 2.013(3)	N(1)–Cu(1)–N(4) 165.04 (12)	Cu(1)–N(3) 1.956(3)	N(1)–Cu(1)–N(5) 95.29(13)
Cu(1)–N(4) 2.027(3)	N(2)–Cu(1)–N(3) 165.10(12)	Cu(1)–N(5) 2.032(3)	N(1)–Cu(1)–N(6) 94.81(12)
	N(2)–Cu(1)–N(4) 82.45(11)	Cu(1)–N(6) 2.255(3)	N(2)–Cu(1)–N(3) 82.54(12)
	N(3)–Cu(1)–N(4) 112.24(12)		N(2)–Cu(1)–N(5) 166.49(12)
			N(2)–Cu(1)–N(6) 117.48(12)
			N(3)–Cu(1)–N(5) 96.95(12)
			N(3)–Cu(1)–N(6) 103.42(12)
			N(5)–Cu(1)–N(6) 75.84(12)

3.3. IR spectra

The IR spectral data of the free ligand (**DPPA**) and the Cu(II) complexes with their relative assignments were studied to characterize their structures. The assignments of the infrared spectra

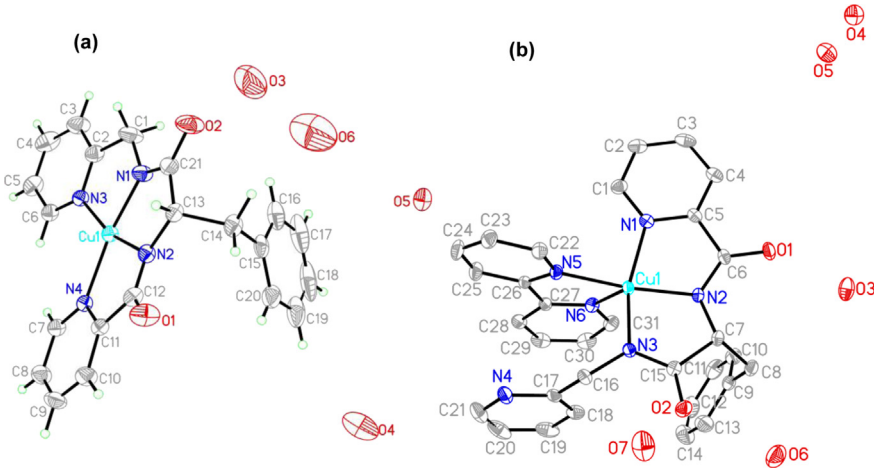

Fig. 2. An ORTEP view of **1** (a) and **2** (b) showing the atom labeling scheme (50% probability thermal ellipsoids).

were made on the basis of literature and Nakamoto [49]. The IR spectra of the complexes were analyzed in comparison with their free ligand spectra (†Fig. S6a–c). In the IR spectra of **1**-**3** (†Fig.S6d–f) a broad peak appeared at 3438, 3425 and 3427 cm^{-1} respectively for **1**–**3** were assigned to the υ(O–H) of water molecules present in the crystal lattice. The IR spectra of ligand exhibited a sharp peak at 3293 cm^{-1} which was attributed to the υ(N–H) vibrations, disappeared in the complexes due to the deprotanation of amide group upon complexation with copper. This indicates that the nitrogen atoms of the amide group coordinated to Cu(II) ion. An intense stretching absorption detected at 1655 cm^{-1} was due to the amide carbonyl group υ(C=O) of **DPPA**, which was shifted to 1643, 1615 and 1618 cm^{-1} in complexes **1**–**3** respectively. The peaks corresponding to the ring stretching frequencies (ν(C=C) and ν(C=N)) at 1579 and 1454 cm^{-1} for free bpy and at 1506 and 1419 cm^{-1} for phen were shifted to 1596 and 1441 cm^{-1} for **2** (1553 and 1428 cm^{-1} for **3**) upon complexation. And the characteristic low energy pyridine ring in and out-of-plane hydrogen bending modes of free bpy observed at 758 and 619 cm^{-1} (850 and 734 cm^{-1} for phen) were shifted to 764 and 703 cm^{-1} for **2** (848 and 730 cm^{-1} for **3**), which is an indication of the coordination of the heterocyclic nitrogen to copper. The new non-ligand peaks at 527, 580 and 583 cm^{-1} for **1**–**3** respectively were assigned to υ(Cu–N) vibration [50], also indicates that the ligands are coordinated to copper through nitrogen atoms.

3.4. UV–vis spectra

The electronic spectra of the Cu(II) complexes (**1**–**3**) recorded in aq. methanol at room temperature show absorption bands with varied intensity. The electronic spectra of **3** was shown in Fig. 3 (†Fig. S7 for **1**and **2**). The intense UV bands at 257 (**1**), 207, 270 (**2**) and 222, 264 nm (**3**) were assigned to intra-ligand (π–π*) transition of **DPPA** and bpy/phen ligands, while the less intense bands in the range 392–395 nm of **1**–**3** were assigned to the LMCT transitions. Besides, in the visible region a broad band (insets of res. Figures) observed at 530 nm for **1** was assigned to $^4\mathbf{A_2} \rightarrow {}^4\mathbf{T_1}$ transition, which suggests that the complex was arranged in a distorted square planar geometry. On the other hand for the complexes **2** and **3** the bands at 690 and 710 nm were due to $^2\mathbf{B_{1g}} \rightarrow {}^2\mathbf{A_{1g}}$ transition supporting an approximate square pyramidal geometry around copper [51].

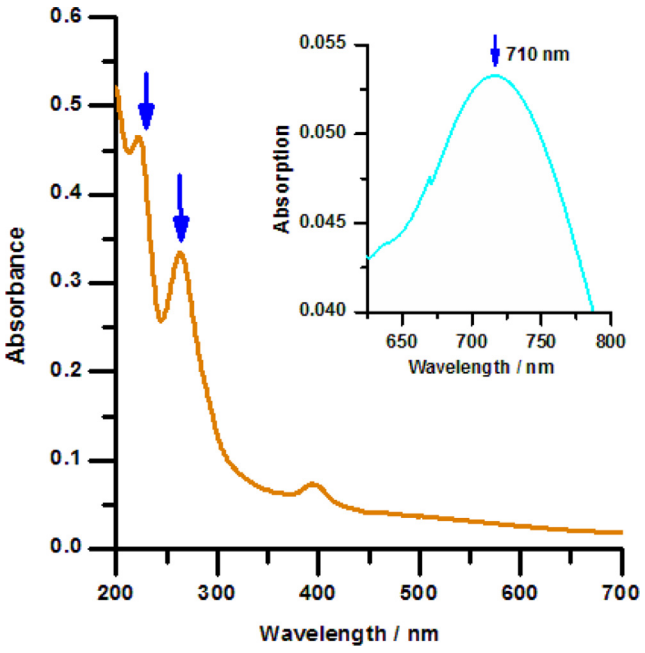

Fig. 3. Electronic absorption spectrsa of **3**. Insets: d–d transition.

3.5. ESI-MS studies

Formation of the ligand (**DPPA**) and its Cu(II) complexes was confirmed by electrospray ionization mass spectrometry (ESI-MS). A peak observed in the **DPPA** spectrum at *m*/*z* 361 (†Fig. S5 c) assigned to the $[M + H]^+$ is of molecular ion species. The ESI-MS spectra of complex **1** show peaks at *m*/*z* 422 $[MH]^+$ and 444 $[M + Na]^+$, complex **2** at *m*/*z* 578 $[M + H]^+$ and complex **3** show peaks at *m*/*z* 602 $[M + H]^+$ and *m*/*z* 624 $[M + Na]^+$. These *m*/*z* values indicate different stiochiometric ratios for the complexes: 1:1 (Cu:DPPA) for **1** and 1:1:1 (Cu:DPPA:bpy and Cu:DPPA:phen) for **2** and **3** respectively.

3.6. DNA binding

DNA is the primary intracellular target of many anticancer drugs [52]. DNA binding is the critical step for DNA cleavage in most cases and has importance in understanding the mechanism of tumor inhibition for the treatment of cancer. Therefore the binding mode and affinity involved between the complexes (**1**–**3**) and CT-DNA was investigated by thermal denaturation, UV–vis absorption spectra, competitive binding, viscosity and fluorescence quenching studies in tris–HCl buffer.

3.6.1. Thermal denaturation

Thermal denaturation experiments were carried out to study the stability of the duplex CT-DNA in the presence of complexes. The interaction of small molecules with double-helical DNA may increase or decrease T_m, the temperature at which the double helix is broken up into a single-stranded DNA. While increase in T_m values suggest an intercalative or phosphate binding, decrease is typical for base binding. The thermal denaturation profile of DNA in

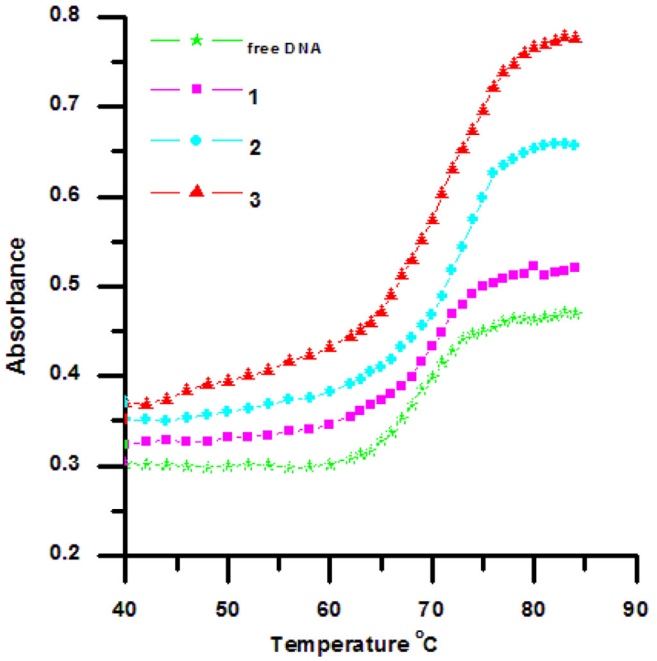

Fig. 4. Thermal denaturation profiles of CT DNA before and after addition of **1**–**3** (30 μM). The DNA concentration was fixed at 30 μM.

Table 4
DNA binding and cleavage data of complexes (**1**–**3**).

	Thermal denaturation		UV–vis absorption			Fluorscence quenching kinetics		
	ΔT_m[a]	λ_{max} (nm)	$\Delta\lambda$	$H\%$[b]	Change in Abs.	K_b[c]	K_{sq}[d]	K_{cat}[e]
(**1**)	4	257	4	14	Hypochromism	8.3×10^4	0.09	2.09
(**2**)	7	270	4	19	Hypochromism	1.23×10^5	0.17	2.45
(**3**)	9	264	6	23	Hypochromism	1.35×10^5	0.25	2.89

[a] T_m of Free DNA − T_m of complex bound to DNA.
[b] Percentage of Hypochromism.
[c] Intrinsic DNA binding constant (M^{-1}).
[d] Stern–Volmer Quenching constant.
[e] DNA cleavage rate constant (h^{-1}).

the absence and presence of complexes **1**–**3** is provided in Fig. 4. As can be seen, an increase of 4–9 °C for **1**–**3** (Table 4) was observed in the T_m profile of complexes as compared to free DNA. The DNA melting data suggest an intercalative/phosphate mode of binding with copper complexes. The ΔT_m values follow the order of **3** > **2** > **1** which is in accordance with their aromaticity.

3.6.2. Interaction of CT DNA with *1*–*3* by UV–vis titration

UV–visible absorption spectral measurements were performed for electronic perturbations for the interaction of complexes with CT-DNA to determine the intrinsic binding constants (K_b) [53]. The absorption spectra of the complex **3** in the absence and presence of increasing amounts of DNA is illustrated in Fig. 5. On the addition of increasing amounts of DNA to the complex **3**, both hypochromic (23%) (14% for **1** 19% for **2**) and bathochromic shifts from 264 to 270 nm (257–261 nm for **1** and 270–274 for **2**) were observed. The hypochromism and bathochromism were suggested to arise due to the interaction between the electronic state of an intercalating chromophore (complex) and those of the DNA bases [54,55]. These results demonstrate that the complex may bind to DNA through an intercalation of the complex into the double helix structure of DNA.

Similar results were obtained for **1** and **2** (†Fig. S8). The intrinsic binding constant (K_b) for the association of the complexes with CT-DNA (insets of res. figures) were determined as $8.3 \pm 0.01 \times 10^4$ M^{-1}, $1.23 \pm 0.01 \times 10^5$ M^{-1} and $1.35 \pm 0.01 \times 10^5$ M^{-1} for complexes **1**–**3** respectively (Table 4) by using Equation (1). The lower binding constant of binary complex (**1**) as compared to ternary complexes (**2** and **3**) is due to the absence of planar heterocyclic bases in the former. The higher DNA binding ability of the phen complex compared to its bpy analogue is due to the presence of an extended aromatic phenyl ring (in phen) which might facilitate partial intercalation of the base moiety through noncovalent π–π interaction with the DNA bases.

3.6.3. Viscosity

The viscosity measurements were carried out on CT-DNA by increasing the concentration of the added complexes and EB, a known DNA intercalator for comparison. The effects of the Cu(II) complexes (**1**–**3**) and EB on the viscosity of CT-DNA was shown in Fig. 6. In the presence of complexes, the viscosity of DNA has been found to increase similar to that of EB, a proven DNA intercalator, suggesting that the complexes bind to DNA through an intercalation. This result is consistent with the classical intercalators [56,57]. The increased degree of viscosity, which may depend on their affinity to DNA follow the order **1** < **2** < **3** < EB. This is attributed to an increase of aromatic planar rings from complexes **1**–**3**.

3.6.4. Competitive binding

Intercalative binding was also demonstrated through competitive binding experiments with EB as an intercalative probe [58] using absorption spectroscopy. The study involves the addition of complexes to DNA pre-treated with EB and recording of the intensity of absorption. On interaction with DNA, free EB which has an absorption maxima ~480 nm was shifted to a higher wavelength followed by a decrease in absorption. This provides a reasonable evidence for the intercalation of EB into the DNA base

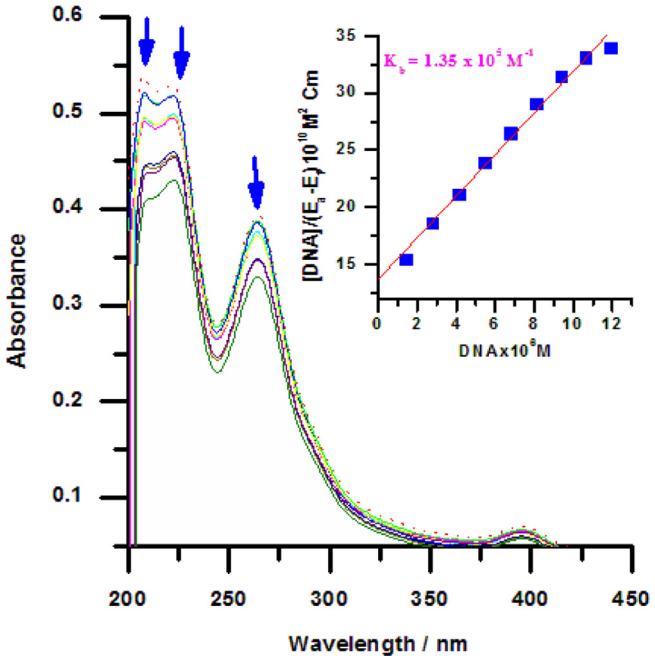

Fig. 5. Absorption spectra of **3** in the absence (.....) and presence (—) of increasing amounts of CT-DNA. Conditions: [Cu] = 10 μM, [DNA] = 0–10 μM. Arrow (↓) shows the absorbance changes upon increasing DNA concentration. Inset: linear plot for the calculation of the intrinsic DNA binding constant, K_b.

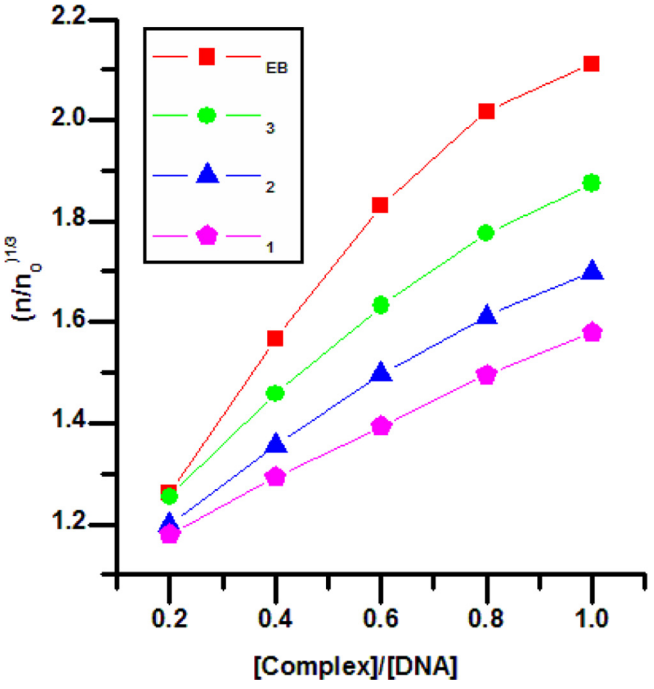

Fig. 6. Effect of increasing amount of EB and complexes **1**–**3** on the relative viscosities of CT-DNA at room temp. in 5 mM Tris–HCl buffer. Conditions: [DNA] = 200 μM, [complex] = 0–120 μM.

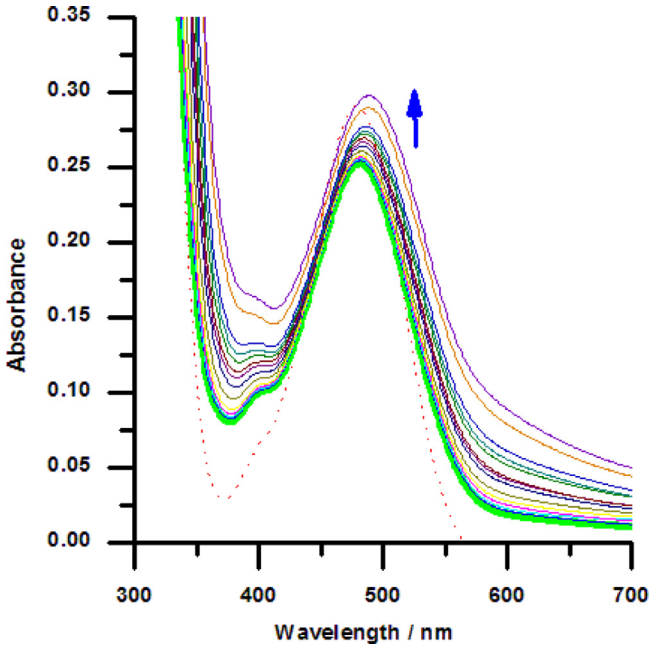

Fig. 7. Absorption spectra of free EB (.....) and EB bound to CT-DNA in the absence (———) and presence (—) of increasing amount of **3**. Conditions: [EB] = 40 μM, [DNA] = 40 μM, [**3**] = (0–40 μM). Arrow (↑) shows the absorbance changes upon increasing complex concentration.

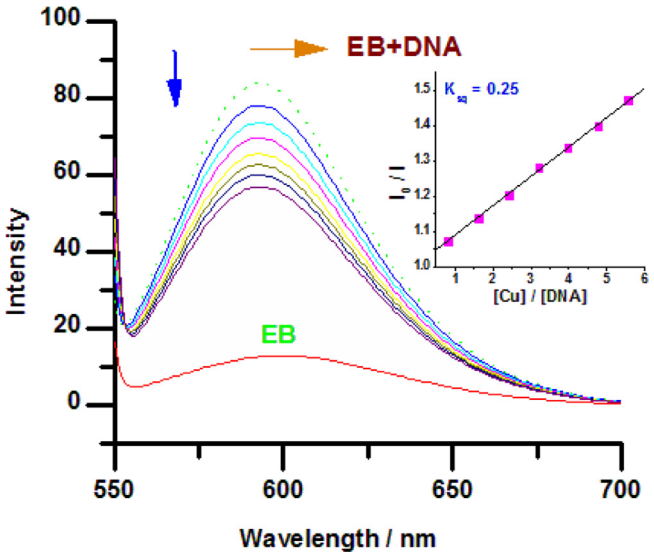

Fig. 8. Emission spectra of EB bound to CT-DNA in the absence (.....) and presence (—) of complex **3**. [**3**/DNA = 0, 0.8, 1.60, 2.41, 3.19, 3.97, 4.78, λ_{ex} = 540 nm, Inset: Stern–Volmer quenching curve].

stacks [59]. Fig. 7 reflects the above conclusion where the absorption maxima of free EB at 478 nm was shifted to 481 nm in the presence of DNA. Addition of **3** to the EB-DNA solution caused an enhancement in the absorption intensity, which is an indication of competitive binding of **3** with EB to bind to DNA. Similar trends were observed for **1** and **2** (†Fig. S9). The results clearly suggest that **1**–**3** bind to DNA through an intercalative mode by the release of intercalatively bound EB. These results are consistent with those obtained from the spectroscopic studies and viscosity measurements.

3.6.5. Fluorescence spectroscopy

The quenching experiments based on the displacement of an intercalating drug EB from CT-DNA will provide further information about the relative binding affinity of the complexes to CT-DNA with respect to EB. The fluorescence quenching curves of EB bound to DNA in the absence and presence of **3** was given in Fig. 8.

It may be seen from the Figure, the EB-DNA system shows characteristic strong emission at about 598 nm when excited at 540 nm, indicating that the intercalated EB molecules have been successfully protected by the hydrophobic environment inside the DNA helix from being quenched by H_2O; as a result the accessibility of solvent molecules to EB is reduced. A remarkable reduction in emission intensity was observed when **3** was added to EB-DNA system, characteristic for the intercalative binding of the complex with DNA. Similar trends were observed for **1** and **2** (†Fig. S10). Some mechanisms have been proposed to account for this reduction in the emission intensity: the replacement of molecular fluorophores [60,61], electron transfer [62], energy transfer [63] and proton transfer [64].

The quenching efficiency for each complex was evaluated by the Stern–Volmer constant K_{sq}, which varies with the experimental conditions, $I_o/I = 1 + K_{sq}.r$; where I_o and I are the fluorescence intensities in the absence and presence of the complex, respectively, and r is the concentration ratio of the complex to DNA. K_{sq} is a linear Stern–Volmer quenching constant. The quenching plots illustrate that the quenching emission of EB-DNA system by the complexes are in good agreement with the linear Stern Volmer equation [65], which also suggest that the complexes are bound to DNA. The K_{sq} value was obtained as the ratio of the slope to intercept. The K_{sq} values for the complexes **1**–**3** are 0.09, 0.17 and 0.25 respectively (insets of respective figures and Table 4).

Fluorescence *Scatchard* plots for the binding of EB to CT-DNA in the presence of the complexes were obtained as described by Lepecq and Paoletti [47]. From the *Scatchard* plots, complexes can be classified as Type A or Type B. In Type A complexes, *Scatchard* plot show decrease in the slope in the presence of increasing amounts of metal complex, with no change in the intercept on the abscissa suggesting a competitive inhibition of ethidium bromide binding (intercalation) [66,67] whereas Type B complexes show a change in slope and intercept, suggesting intercalative and covalent interactions with DNA [68,69]. The binding isotherms of EB and DNA in the absence and presence of **1**–**3** were determined experimentally and presented in Fig. 9. As can be seen from the plots a decrease in slope with no change in the intercept was observed upon the addition of **1**–**3** indicating an intercalative mode of binding of the complexes with DNA. These results also concur with those obtained from other techniques viz. absorption, viscosity and emission spectral studies.

In summary, the DNA binding studies revealed that the binding of **1**–**3** to CT-DNA was through an intercalation.

3.7. DNA cleavage

Natural plasmid DNA mainly has a closed circle supercoiled form (SC), and nicked circular (NC) and linear forms (LC) as small fractions. Relaxation of supercoiled pUC19 DNA into nicked circular and linear conformation was used to quantify the relative cleavage efficiency of the complexes (**1**–**3**) by agarose gel electrophoresis technique. At neutral pH, DNA is negatively charged so it moves through the gel from cathode towards anode. It is also a useful technique to investigate various binding modes of small molecules to SC DNA. Intercalation of small molecules to plasmid DNA can loosen or cleave the SC DNA form, which results in the decrease of its (SC DNA) mobility rate and can be separately visualized by agarose gel electrophoresis method. The gel electrophoretic

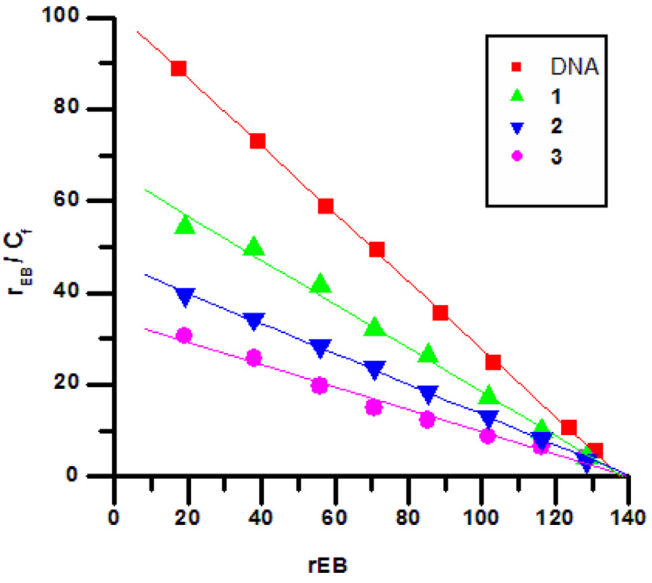

Fig. 9. Fluorescence *Scatchard* plots for the EB bound to CT-DNA in the absence (■) and presence of **1** (▲), **2** (▼) and **3** (●). The term r_{EB} is the concentration ratio of bound EB to total DNA, and c_f is the concentration of free EB.

mobility assay (Fig. 10) reveal the conversion of supercoiled (SC) plasmid pUC19 DNA into nicked circular (NC) form by complexes **1**–**3**. For DNA cleavage experiments its concentration was 38 μM base pairs.

3.7.1. Oxidative cleavage

The ability of the complexes **1**–**3** in inducing oxidative DNA cleavage was studied. On reaction with SC DNA in the presence of hydrogen peroxide (H_2O_2), all complexes show efficient nuclease activity (Fig. 10a; lanes 7–10 for **1**; Fig. 10b lanes 8–10 for **2** and Fig. 10c lanes 8–11 for **3**). Control experiment with only H_2O_2 (lane 7) does not show any appreciable DNA cleavage (<10%), but in the presence of complexes **1**–**3** the SC DNA was totally converted to NC form. Total conversion of SC to NC form was achieved by complex **1** at a concentration of 10 μM where as only 5 μM was required for complexes **2** and **3**. Total inhibition of cleavage was observed in the presence of DMSO, a hydroxyl radical scavenger. This indicates the possible involvement of hydroxyl radical and/or the reactive copper-oxo species in the cleavage pathway. On the basis of this observation, the mechanism of DNA cleavage mediated by **1**–**3** may be proposed as follows: DNA cleavage is redox-mediated – The complexes would first interact with DNA through intercalation to form a Cu(II)—DNA adduct species followed by its reduction by the external agent (H_2O_2) to a Cu(I)—DNA system, which then

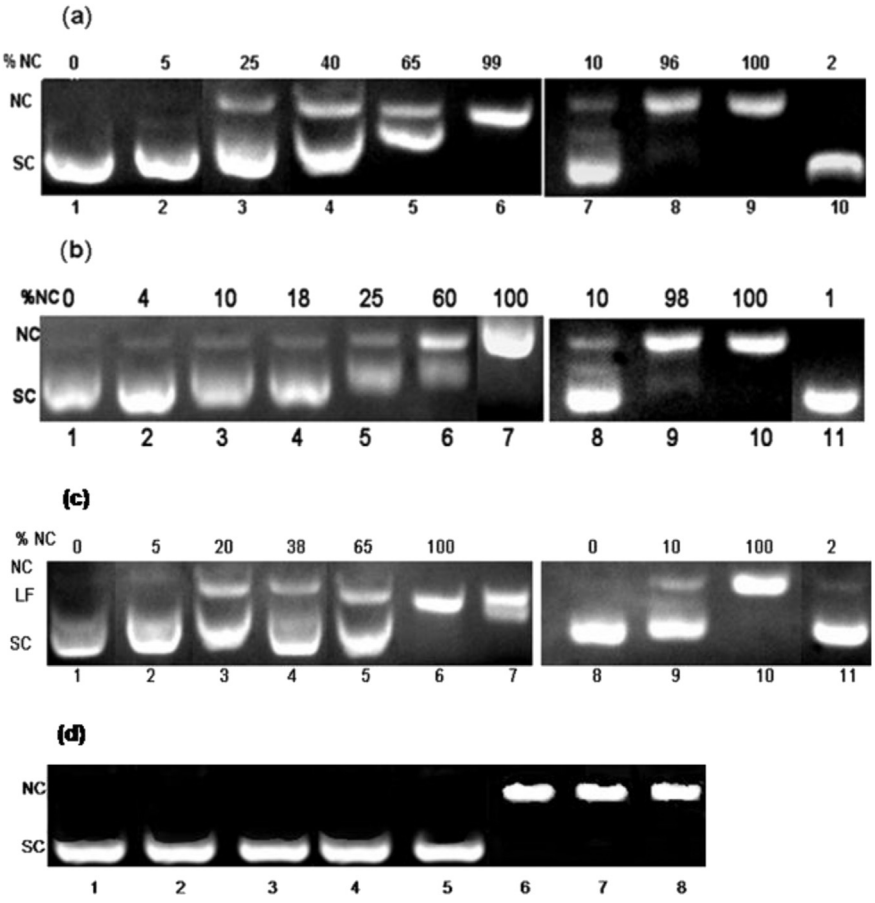

Fig. 10. Agarose gel electrophoresis pattern for the cleavage of supercoiled pUC19 DNA (38 μM base pairs concentration) by **1** and **2** at 37 °C in a buffer containing 5 mM tris. HCl/5 mM aq.NaCl. (a) Lane 1, DNA control; Lane 2, DNA + **1**(10 μM); Lane 3, DNA + **1**(25 μM); Lane 4, DNA + **1**(50 μM); Lane 5, DNA + **1**(75 μM); Lane 6, DNA + **1**(100 μM); Lane 7, DNA + H_2O_2 (1 mM); Lane 8, DNA + **1**(5 μM) + H_2O_2 (1 mM); Lane 9, DNA + **1**(10 μM) + H_2O_2 (1 mM); Lane 10, DNA + **1**(10 μM) + H_2O_2 (1 mM) + DMSO (1 mM). (b) Lane 1, DNA control; Lane 2, DNA + **2**(5 μM); Lane 3, DNA + **2**(10 μM); Lane 4, DNA + **2**(20 μM); Lane 5, DNA + **2**(40 μM); Lane 6, DNA + **2**(60 μM); Lane 7, DNA + **2**(80 μM); Lane 8, DNA + H_2O_2 (1 mM); Lane 9, DNA + **2**(5 μM) + H_2O_2 (1 mM); Lane 10, DNA + **2**(10 μM) + H_2O_2 (1 mM); Lane 11, DNA + **2**(10 μM) + H_2O_2 (1 mM) + DMSO (1 mM). (c) Lane 1, DNA control; Lane 2, DNA + **3**(5 μM); Lane 3, DNA + **3**(10 μM); Lane 4, DNA + **3**(20 μM); Lane 5, DNA + **3**(40 μM); Lane 6, DNA + **3**(60 μM); Lane 7, DNA + **3**(80 μM); Lane 8, DNA control; Lane 9, DNA + H_2O_2 (1 mM); Lane 10, DNA + **3**(5 μM) +H_2O_2 (1 mM). (d) Lane 1, DNA control; Lane 2, DNA + $Cu(OAc)_2$(1 mM); Lane 3, DNA + DPPA(1 mM); Lane 4, DNA + bpy (1 mM); Lane 5, DNA + phen (1 mM); Lane 6, DNA + **1**(100 μM) + DMSO (1 mM); Lane 7, DNA + **2**(80 μM) + DMSO (1 mM); Lane 8, DNA + **3** (60 μM) + DMSO (1 mM).

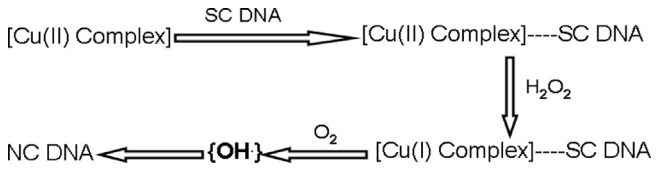

Scheme 2. A possible mechanism for the oxidative cleavage of DNA by **1**–**3** in the presence of H_2O_2.

generates hydroxyl radicals on reaction with O_2. These hydroxyl radicals would then attack DNA, causing strand scission (Scheme 2). This pathway was proposed by Sigman and co-workers for the oxidative cleavage reaction of the bis(phen)copper complex [70] which is the most accepted one.

3.7.2. Hydrolytic cleavage

Attempts were also made to cleave DNA through hydrolysis of phosphodiester bond. Since this process does not require any external agents and light it has biological relevance. When DNA was incubated with increasing concentrations of complexes SC DNA was degraded to NC form. The catalytic activities of **1**–**3** are depicted in Fig. 10. All complexes start their activity at a conc. as low as 10 μM. At 100 μM a complete conversion of supercoiled plasmid DNA into the nicked circular form was observed for **1** (Fig. 10a; lane 6). In contrast complete conversion was achieved at 80 μM (Fig. 10b; lane 7) for **2** and at 60 μM for **3** (Fig. 10c; lane 6); on increasing the concentration of **3**–100 μM further conversion of the NC form to linear form (LF) was observed (Fig. 10c; lane 7). As can be seen from the above results the hydrolysis of DNA follows the order **1** < **2**<**3**, this is due to the extended planar aromatic moieties in **1**–**3** which can insert deeply in to the bases of DNA.

To ensure that the copper complexes are solely responsible for the cleavage, several control experiments were performed under identical conditions (Fig. 10d). No cleavage of DNA was observed with free copper and free ligands (1 mM). In a control experiment with DMSO (1 mM), a known radical scavenger, only slight inhibition (<2%>) of DNA cleavage was observed. This rule-out the possibility of DNA cleavage via $OH^{\bullet}$-based depurination pathway and also a possible oxidative cleavage [71] (dioxygen + copper complex + traces of DNA). This suggests that the DNA cleavage was the result of hydrolysis of a phosphodiester bond. Thus, the present study reveals that no diffusable radical is involved in the DNA cleavage as no external agents like H_2O_2, MPA, ascorbic acid or light were employed in the cleavage experiments.

3.7.3. Kinetics

The cleavage of pUC19 DNA by **1**–**3** was kinetically monitored by quantification of SC and NC forms of DNA. The observed distribution of SC and NC DNA in agarose gel provides a measure of the extent of hydrolysis of the phosphodiester bond in each plasmid DNA, and the data were used to perform simple kinetics. The kinetic plots (Fig. 11 for **3** and †Fig. S11 for **1** and **2**) which show a decrease of SC and an increase of NC forms of DNA versus time, follow the pseudo-first-order kinetics and both the forms fitted well to a single exponential curve. From these curve fits, the DNA hydrolysis rates were determined as 2.09 h^{-1} ($R = 0.985$), 2.45 h^{-1}($R = 0.963$) and 2.89 h^{-1} ($R = 0.987$) for **1**–**3** respectively. The enhancement of DNA hydrolysis rate constant by metal complexes in the range of 0.09–0.25 h^{-1} was considered impressive. [83] With the rate constants of 2.09 (**1**), 2.45 (**2**) and 2.89 h^{-1} (**3**) it amounts to an order of (5.8–8.0) × 10^7 fold rate enhancement compared to non-catalyzed double stranded DNA (3.6 × 10^{-8} h^{-1}) [72].

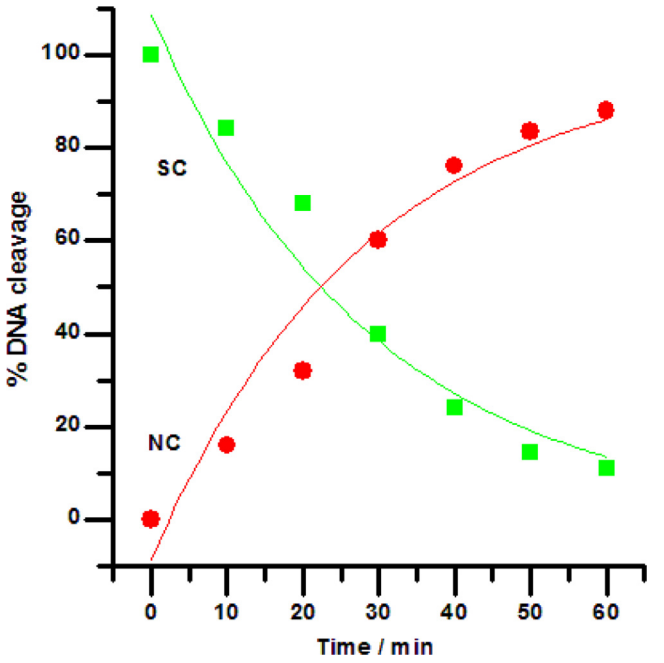

Fig. 11. Disappearance of supercoiled form (SC) DNA and formation of nicked circular (NC) form in the presence of complex **3**. Conditions: [complex] = 100 μM. Data points (■) refer to SC DNA and data points (●) refer to NC DNA.

4. Conclusions

In view of the importance of picolinic acid in preventing cell growth and arresting cell cycle, we have successfully isolated three new picolinic acid based copper(II) complexes [Cu(II)(DPPA)].4H_2O (**1**), [Cu(II)(DPPA)(bpy)].5H_2O (**2**) and [Cu(II)(DPPA)(phen)].5H_2O (**3**) and structurally characterized. Single crystal x-ray structures were determined for complexes **1** and **2**. The complexes arranged in square planar geometry for **1** and square pyramidal geometry for **2** & **3**. Interestingly, the ligand behaves as a tetradentate in square planar complex and tridentate in square pyramidal complexes. The DNA binding studies revealed that they bind to CT DNA in an intercalative mode of interaction. The binding constants decrease in the order **3** > **2** > **1** which was attributed to the increasing aromaticities of the complexes. The complexes exhibit efficient nuclease activity towards supercoiled pUC19 DNA. The cleavage activity of the complexes increase in the order **1** < **2** < **3**. The studies suggest the DNA cleavage was carried out by involvement of hydroxyl radical in the oxidative pathway, whereas in the hydrolytic cleavage hydroxyl radical was not generated. The present Cu(II) complexes are solely responsible for hydrolytic cleavage. The kinetic data indicate that the cleavage reactions follow pseudo first order rate constants and the rates for the cleavage of DNA phosphodiester bond are impressive. Thus, the picolinic acid based ligands with increased aromaticities may be developed as DNA recognition elements in designing efficient metal based anticancer agents.

Acknowledgments

The financial support to PRR from the Council of Scientific and Industrial Research (Grant No. 01/2569/12- EMR- II) and University Grants Commission (Grant No. 41- 286/2012 (SR)), Govt. of India is gratefully acknowledged. NR thanks CSIR for Senior Research Fellowship.

Abbreviations

DPPA	pyridine-2-carboxylic acid {2-phenyl-1-[(pyridin-2-ylmethyl)-carbonyl]-ethyl}-amide
PA	picolinic acid
bpy	2,2′-Bipyridine
phen	1,10-Phenanthroline
CT-DNA	calf-thymus deoxyribonucleic acid
FT-IR spectra	Fourier transform Infrared spectra
UV–vis	ultraviolet visible
ESI-MS	electrospray ionization mass spectra
EB	ethidium bromide
MeOH	methanol
DMSO	dimethyl sulfoxide
SC DNA	supercoiled deoxyribonucleic acid
NC	nicked circular

Appendix A. Supplementary data

Supplementary data related to this article can be found at http://dx.doi.org/10.1016/j.ejmech.2014.03.084.

References

[1] L.J. Boerner, J.M. Zaleski, Current Opinion in Chemical Biology 9 (2005) 135–144.
[2] Y.W. Jung, S.J. Lippard, Chemical Reviews 107 (2007) 1387–1407.
[3] S.E. Sherman, S.J. Lippard, Chemical Reviews 87 (1987) 1153–1181.
[4] A.S. Abu-Surrah, M. Kettunen, Current Medicinal Chemistry 13 (2006) 1337–1357.
[5] E.R. Jamieson, S.J. Lippard, Chemical Reviews 99 (1999) 2467–2498.
[6] S. Dhar, D. Senapati, P.K. Das, P. Chatopadhyay, M. Nethaji, A.R. Chakravarty, Journal of the American Chemical Society 125 (2003) 12118–12124.
[7] H. Prakash, A. Shodal, H. Yasul, H. Sakural, S. Hirota, Inorganic Chemistry 47 (2008) 5045–5047.
[8] D. Li, J. Tian, Y. Kou, F. Huang, G. Chen, W. Gu, X. Liu, D. Liao, P. Cheng, S. Yan, Dalton Transactions (2009) 3574–3583.
[9] Y. Sun, L.E. Joyce, N.M. Dickson, C. Turro, Chemical Communications 46 (2010) 2426–2428.
[10] A. Jain, J. Wang, E.R. Mashack, B.S.J. Winkel, K.J. Brewer, Inorganic Chemistry 48 (2009) 2711–2718.
[11] L.A. Mullice, R.H. Laye, L.P. Harding, N.J. Buurma, S.J.A. Pope, New Journal of Chemistry 32 (2008) 2140–2149.
[12] L.Z. Li, C. Zhao, T. Xu, H.W. Ji, Y.H. Yu, G.Q. Guo, H. Chao, Journal of Inorganic Biochemistry 99 (2005) 1076–1082.
[13] J. Reedijk, in: G. Wilkinson, R.D. Gillard, J.A. McCleverty (Eds.), Heterocyclic Nitrogen-donor Ligands Comprehensive Coordination Chemistry, vol. 2, Pergamon Press, Oxford, 1987, p. 73 (and references therein).
[14] D.A. House, doi:10.1039/C2DT30512G Comprehensive Coordination Chemistry, in: G. Wilkinson, R.D. Gillard, J.A. McCleverty (Eds.), Ammonia and Amines, vol. 2, Pergamon Press, Oxford, 1987, p. 23 (and references therein).
[15] F. Grob, A. Müller-Hartmann, H. Vahrenkamp, European Journal of Inorganic Chemistry 11 (2000) 2363–2370.
[16] W.L. Driessen, R.A.G. Graaf, F.J. Parevliet, J. Reedijk, R.M. de Vos, Inorganica Chimica Acta 216 (1994) 43–49.
[17] S. Wang, Q. Luo, X. Wang, L. Wang, K. Yu, Journal of the Chemical Society, Dalton Transactions (1995) 2045–2055.
[18] H. Adams, N.A. Bailey, J.D. Crane, D.E. Fenton, J.M. Latour, J.M. Williams, Journal of the Chemical Society, Dalton Transactions (1990) 1727–1735.
[19] T. Bortolotto, P.P. Silva, A. Neves, E.C. Pereira-Maia, H. Terenzi, Inorganic Chemistry 50 (2011) 10519–10521.
[20] T. Hirohama, Y. Kuranuki, E. Ebina, T. Sugizaki, H. Arii, M. Chikira, P. Tamil Selvi, M. Palaniandavar, Journal of Inorganic Biochemistry 99 (2000) 1205–1219.
[21] S. Anbu, S. Shanmugaraju, M. Kandaswamy, RSC Advances 2 (2012) 5349–5357.
[22] F. He, L. Tao, X. Li, Y. Li, Z. Wu, C. Yan, New Journal of Chemistry 36 (2012) 2078–2087.
[23] P.R. Reddy, K.S. Rao, B. Satyanarayana, Tetrahedron Letters 47 (2006) 7311–7315.
[24] P.R. Reddy, P. Manjula, Chemistry and Biodiversity 4 (2007) 468–480.
[25] P.R. Reddy, P. Manjula, T.K. Chakraborty, R. Samanta, Chemistry and Biodiversity 6 (2009) 764–773.
[26] P.R. Reddy, A. Shilpa, Indian Journal of Chemistry 49A (2010) 1003–1015.
[27] P.R. Reddy, A. Shilpa, Polyhedron 30 (2011) 565–572.
[28] P.R. Reddy, A. Shilpa, N. Raju, P. Raghavaiah, Journal of Inorganic Biochemistry 105 (2011) 1603–1612.
[29] P.R. Reddy, N. Raju, B. Satyanarayana, Chemistry and Biodiversity 8 (2011) 131–144.
[30] P.R. Reddy, N. Raju, Polyhedron 44 (2012) 1–10.
[31] G. Frumento, R. Rotondo, M. Tenetti, G. Domonte, U. Benatti, G.B. Ferrara, Journal of Experimental Medicine 196 (2002) 459–468.
[32] J.A. Fernadez-pol, D.J. Klos, P.D. Hamilton, Anticancer Research 21 (2001) 3773.
[33] (a) P. Srinivas, P.R. Likhar, H. Maheswaran, B. Sridhar, K. Ravikumar, M. Lakshmi Kantam, Chemistry – European Journal 15 (2009) 1578–1581; (b) M. Bodanszky, A. Bodanszky, The Practices of Peptide Synthesis, Springer, New York, 1984.
[34] B.N. Figgi's, J. Lewis, in: J. Lewis, R.C. Wilkinson (Eds.), Modern Coordination Chemistry, Wiley Interscience, New York, 1967.
[35] SMART Version 5.630, SAINT-plus Version 6.45, Programs for Data Collection and Extraction, Bruker-Nonius Analytical X-ray Systems Inc., Madison, WI, USA, 2003.
[36] G.M. Sheldrick, SADABS: Program for Empirical Absorption Correction, University of Gottingen, Gottingen, Germany, 1997.
[37] G.M. Sheldrick, SHELX-97: Programs for Structure Solution and Refinement, University of Gottingen, Gottingen, Germany, 1997.
[38] L.J. Farrugia, Journal of Applied Crystallography 32 (1999) 837–838.
[39] P. McArdle, Journal of Applied Crystallography 28 (1995) 65.
[40] A.L. Spek, PLATON: a Multipurpose Crystallographic Tool, Utrecht University, Utrecht, The Netherlands, 2002.
[41] J. Marmur, Journal of Molecular Biology 3 (1961) 208–218.
[42] M.E. Reichmann, C.A. Rice, C.A. Thomos, P. Doty, Journal of the American Chemical Society 76 (1954) 3047–3053.
[43] F. Garland, D.E. Graves, L.W. Yielding, H.C. Cheung, Biochemistry 19 (1980) 3221–3226.
[44] J. He, P. Hu, Y. Wang, M. Tong, H. Sun, Z. Mao, L. Ji, Dalton Transactions (2008) 3207–3214.
[45] C.V. Kumar, E.H. Asuncion, Journal of the American Chemical Society 115 (1993) 8547–8553.
[46] A. Wolfe, G.H. Shimer, T. Meehan, Biochemistry 26 (1987) 6392–6396.
[47] J.B. Lepecq, C.J. Paoletti, Journal of Molecular Biology 27 (1967) 87–106.
[48] R.N. Patel, N. Singh, V.L.N. Gundla, Indian Journal of Chemistry 45A (2006) 614–618.
[49] K. Nakamoto, Infrared and Raman Spectra of Inorganic and Coordination Compounds, third ed, John Wiley & Sons, New York, p. 228.
[50] G.G. Mohamed, M.M. Omar, A.M.M. Hindy, Spectrochimica Acta, Part A 62 (2005) 1140–1150.
[51] A.B.P. Lever, Inorganic Electronic Spectroscopy, Elsevier, New York, 1984.
[52] M. Chauhan, K. Banerjee, F. Arjmand, Inorganic Chemistry 46 (2007) 3072–3082.
[53] J.M. Kelly, A.B. Tossi, D.J. McConnell, C. OhUigin, Nucleic Acids Research 13 (1985) 6017–6034.
[54] M. Navarro, E.J. Cisneros-Fajardo, A. Sierralta, M. Fernández-Mestre, P. Silva, D. Arrieche, E. Marchán, Journal of Biological Inorganic Chemistry 8 (2003) 401–408.
[55] H.M. Berman, P.R. Young, Annual Review of Biophysics and Bioengineering 10 (1981) 87–114.
[56] H. Deng, H. Xu, Y. Yang, H. Li, H. Zou, L.H. Qu, L.N. Ji, Journal of Inorganic Biochemistry 97 (2003) 207–214.
[57] C.Y. Zhou, X.L. Xi, P. Yang, Biochemistry (Moscow) 72 (2007) 37–43.
[58] D.-D. Qin, Z.-Y. Yang, B.D. Wang, Spectrochimica Acta Part A 68A (2007) 912–917.
[59] W.D. Wilson, L. Ratmeyer, M. Zhao, L. Strekowski, D. Boykin, Biochemistry 32 (1993) 4098–4104.
[60] Y.Z. Ma, H.J. Yin, K.Z. Wang, Journal of Physical Chemistry B 113 (2009) 11039–11047.
[61] Y. Lu, L.H. Gao, M.J. Han, K.Z. Wang, European Journal of Inorganic Chemistry (2006) 430–436.
[62] P. Lincoln, E. Tuite, B. Nordén, Journal of the American Chemical Society 119 (1997) 1454–1455.
[63] I. Haq, P. Lincoln, D. Suh, B. Nordén, B.Z. Chowdhry, J.B. Chaires, Journal of the American Chemical Society 117 (1995) 4788–4796.
[64] C. Turro, S.H. Bossmann, Y. Jenkins, J.K. Barton, N.J. Turro, Journal of the American Chemical Society 117 (1995) 9026–9032.
[65] J.R. Lakowicz, G. Webber, Biochemistry 12 (1973) 4161–4170.
[66] H. Arkawa, R. Ahmad, M. Naoui, H.A. Tajmir-Riahi, Journal of Biological Chemistry 275 (2000) 10150–10153.
[67] M. Howe-Grant, K.C. Wu, W.R. Bauer, S.J. Lippard, Biochemistry 15 (1976) 4339–4346.
[68] E. Gao, L. Liu, M. Zhu, Y. Huang, F. Guan, X. Gao, M. Zhang, L. Wang, W. Zhang, Y. Sun, Inorganic Chemistry 50 (2011) 4732–4741.
[69] Z.-F. Chen, L. Mao, L.-M. Liu, Y.-C. Liu, Y. Peng, X. Hong, H.-H. Wang, H.-G. Liu, H. Liang, Journal of Inorganic Biochemistry 105 (2011) 171–180.
[70] D.S. Sigman, Accounts of Chemical Research 19 (1986) 180–186.
[71] R. Ren, P. Yang, W. Zheng, Z. Hua, Inorganic Chemistry 39 (2000) 5454–5463.
[72] A. Roigk, R. Hettich, H.-J. Schneider, Inorganic Chemistry 37 (1998) 751–756.